A Layered Red-Emitting Chromophoric Organic Salt

ARTICLE *in* CRYSTAL GROWTH & DESIGN · AUGUST 2008

Impact Factor: 4.89 · DOI: 10.1021/cg800122v

CRYSTAL GROWTH & DESIGN
2008
VOL. 8, NO. 8
3004–3009

A Layered Red-Emitting Chromophoric Organic Salt

Chenyi Yi,[†] Carmen Blum,[†] Shi-Xia Liu,*[,†] Ying-Fen Ran,[†] Gabriela Frei,[†] Antonia Neels,[‡] Helen Stoeckli-Evans,[‡] Gion Calzaferri,[†] Samuel Leutwyler,[†] and Silvio Decurtins[†]

Departement für Chemie und Biochemie, Universität Bern, Freiestrasse 3, CH-3012 Bern, Switzerland, and Institut de Microtechnique, Université de Neuchâtel, Rue Jaquet Droz 1, CH-2002 Neuchâtel, Switzerland

Received January 31, 2008; Revised Manuscript Received April 25, 2008

ABSTRACT: We have investigated a synthetic route as well as the molecular assembly and the optical properties of a novel π-conjugated system, namely, the anion (*E*)-3-(3-amino-2,4-dicyanophenyl)-1,1-dicyanoprop-2-en-1-ide, in the form of its tetrabutylammonium salt (**1**). Through the combined actions of directional hydrogen bonds and Coulombic interactions, a two-dimensional molecular topology is realized whereby the extended monolayers of the strongly chromophoric π-conjugated anions are spatially isolated by the tetrabutylammonium cations. The chromophoric properties of the anion originate from very intense low-energy $\pi-\pi^*$ absorptions, with a high oscillator strength, $f_{exp} = 0.84$ at 468 nm. Further characteristic features are a $S_1 \rightarrow S_0$ fluorescence emission not only in solution but also in the solid state at room temperature. The remarkable type of organization of the organic chromophores into a solid state sheet structure suppresses a possible quenching of a solid state emission and, quite interestingly, allows in principle probing of the photoexcited exciton states based on a defined molecular geometry.

Introduction

Careful selection of molecules containing functional groups which assemble in the solid state through combined actions of hydrogen bonds and Coulombic interactions allows the construction of robust molecular architectures exhibiting a diverse variety of motifs.[1] Above all, the highly selective and directional nature of hydrogen bonds gives rise to extensive and complex hydrogen bond networks,[2] and in the case of some specifically selected molecular components, preferentially two-dimensional layer structures can be formed, often in a nearly predictable manner.[3] In other words, the reproducible structural control of the self-assembly process on a molecular level lies at the heart of the crystal engineering discipline. We now turn to the concept of combining the power of hydrogen-bond-directed supramolecular interactions with the advantages of extended π-conjugated systems, which can provide functional materials with valuable structural architectures.

Our interest in the design and synthesis of various extended π-conjugated molecular backbones[4] prompted us to explore a new type of a planar functional molecule exhibiting intense chromophoric properties. Consequently, this study seeks to evaluate an interesting synthetic sequence for the preparation of the novel planar, π-extended molecule, which, characteristically, bears a negative charge and a range of functional substituents (Scheme 1). Essentially, the incorporation of dicyanoaniline to 1,1-dicyanoprop-2-en-1-ide brings about a stable and extensively π-conjugated anion, forming a planar molecular structure. As a focal point of this study, this molecule offers a spatially preorganized hydrogen bond donor/acceptor sequence, where the amine group is the hydrogen bond donor and the cyano groups function as hydrogen bond acceptors. In combination, these are favorable prerequisites to realize molecular layered materials based on a two-dimensional hydrogen-bonded network. Specifically, the actual substitution pattern of the anionic skeleton allows the formation of a planar extended ribbon-type motif within the resulting anionic sheets. Since the π-conjugated moieties are negatively charged, the two-dimensional anionic layers tend to assemble in the third dimension, due to Coulombic interactions with appropriate cations, in a densely packed sandwich-type structure. Altogether, this structure represents a rare case of an assembly where the π-conjugated chromophoric units are not packed in a stacking or herringbone motif as it is often the case in so-called *J*- and *H*-aggregates.[5]

Scheme 1. Drawing of the Novel π-Conjugated Anion (*E*)-3-(3-Amino-2,4-dicyanophenyl)-1,1-dicyanoprop-2-en-1-ide

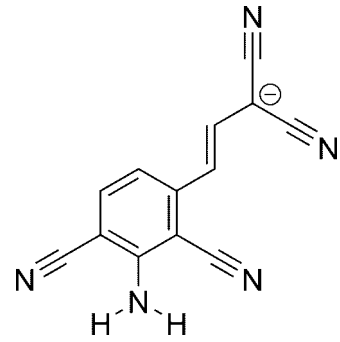

As a result of the extended π-conjugation, strong $\pi-\pi^*$ transitions in the visible spectral region characterize this anion as an organic chromophore, analogous to dye molecules. It is well established that for chromophores assembled in crystals, thin films or molecular aggregates, exciton effects may be observed due to the interactions of the individual chromophores.[6] The resultant exciton couplings may be apparent through spectral shifts of the electronic absorption bands for the component molecules. Thereby, the geometry of the molecular assembly, or more precisely, the size and the relative orientation of the electronic transient dipole moments of the chromophores in the asymmetric unit are the decisive parameters. Moreover, the herein presented novel anionic chromophores which are embedded within the specific 2D salt structure of **1** show at room temperature a solid state fluorescence emission in the red part of the spectrum. This is an interesting aspect because organic fluorophores with strong solid-emissive properties are rare.[7] In

* To whom correspondence should be addressed. E-mail: liu@iac.unibe.ch.
[†] Universität Bern.
[‡] Université de Neuchâtel.

10.1021/cg800122v CCC: $40.75
Published on Web 06/26/2008

most cases, a fluorescence quenching in the molecular aggregation states occurs.

Experimental Section

Reagents and Physical Measurements. 1,5-Bis(trimethylsilyl)penta-1,4-diyn-3-one and 2-amino-4-(trimethylsilyl)-6-(trimethylsilylethynyl)-isophthalonitrile were prepared according to the literature procedures.[8] All other chemicals and solvents were purchased from commercial sources and were used without further purification. All ^{1}H NMR and ^{13}C NMR spectra were measured at 300 and 75.5 MHz, respectively. Chemical shifts, δ, were calibrated against TMS as an internal standard. FT-IR data were collected on a Perkin-Elmer Spectrum One spectrometer. UV−vis absorption and emission spectra were recorded on a Perkin-Elmer Lambda 900 spectrometer and a Perkin-Elmer Luminescence spectrometer LS 50B. Mass spectra were recorded with an Applied Biosystems/Sciex QTrap for the ESI.

Synthesis of Tetrabutylammonium (*E*)-3-(3-Amino-2,4-dicyanophenyl)-1,1-dicyanoprop-2-en-1-ide (1). To a THF (5.0 mL) solution of 2-amino-4-(trimethylsilyl)-6-(trimethylsilylethynyl)isophthalonitrile (168.0 mg, 0.53 mmol), malononitrile (35.6 mg, 0.53 mmol) was added followed by the addition of tetrabutylammonium fluoride solution (1.06 mL, 1 M in THF). The resulting yellow solution was stirred for 2 h at r.t. before the addition of water. Then, the solution was extracted with CH_2Cl_2 (3 × 10.0 mL). The combined organic layer was dried over $MgSO_4$, concentrated under reduced pressure. The residue was purified on a basic alumina (CH_2Cl_2) column to afford **1** as an orange solid. Yield 173.1 mg (68%). mp 128−130 °C. ^{1}H NMR ($CDCl_3$) δ 7.12 (d, J = 8.7 Hz, 1H), 7.11 (d, J = 14.4 Hz, 1H), 6.67 (d, J = 8.7 Hz, 1H), 5.91 (d, J = 14.4 Hz, 1H), 3.15 (m, 8H), 1.61 (m, 8H), 1.41 (m, 8H), 0.98 (t, 12H); ^{13}C NMR ($CDCl_3$) δ 152.51, 148.57, 140.57, 133.76, 117.70, 116.52, 110.37, 102.25, 88.98, 85.82, 58.26, 23.32, 19.19, 13.12. Selected IR data (cm^{-1}, KBr pellet): 3412, 3346, 2960, 2874, 2204, 2179, 2158, 1651, 1545, 1481, 1278, 1186. ESI-MS (negative) m/z 232.2.

X-ray Crystallography. Red-colored crystals with a formula of **1**·0.5CH_3OH were obtained in a rod-shaped morphology by slow evaporation of a solution of **1** in CH_2Cl_2/CH_3OH. The intensity data were collected at −100 °C on a Stoe Mark II-Image Plate Diffraction System[9] equipped with a two-circle goniometer and using Mo Kα graphite monochromated radiation (λ = 0.71073 Å). Image plate distance 130 mm, ω rotation scans 0−180° at ϕ = 0°, and 0−18° at ϕ = 90°, step $\Delta\omega$ = 1.0°, exposures of 5 min per image, 2θ range 1.76−52.59°, $D_{max} - D_{min}$ = 23.107−0.802 Å. The structure was solved by direct methods using the program SHELXS-97.[10] The refinement and all further calculations were carried out using SHELXL-97.[10] The H-atoms, except for those of the amino group, were included in calculated positions and treated as riding atoms using SHELXL default parameters. The non-H atoms were refined anisotropically, using weighted full-matrix least-squares on F^2. An empirical absorption correction was applied using the MULscanABS routine in PLATON;[11] transmission factors: T_{min}/T_{max} = 0.949/0.991. Cell data: monoclinic space group $P2_1/c$, a = 21.8351(15) Å, b = 15.5180(6) Å, c = 19.7104(12) Å, β = 116.585 (5)° V = 5972.5(6) Å^3, fw = 490.71 ($C_{29.5}H_{44}N_6O_{0.5}$), Z = 8, D_{calc} = 1.091 g·cm^{-3}, μ = 0.067 mm^{-1}. Final R indices [$I > 2\sigma(I)$], R_1 = 0.0612, wR_2 = 0.1444, GOF = 0.938 for 11 259 reflections and 674 parameters and R indices (all data), R_1 = 0.1173, wR_2 = 0.1656.

Results and Discussion

Crystal Structure. The compound crystallizes as the solvated compound **1**·0.5CH_3OH in the centrosymmetric monoclinic space group $P2_1/c$. The asymmetric unit comprises two tetrabutylammonium cations, two anions, and one molecule of methanol and all atoms lie on general positions. The ORTEP drawings of the two crystallographically independent anions are shown in Figure 1. The anions form virtually planar, extended π-systems (rms deviation from a least-squares plane through all atoms amounts for the C1 containing anion to only 0.130 Å; maximum deviation for N4: 0.317(2) Å; and for the C14 containing anion to only 0.084 Å; maximum deviation for C15: 0.175(2) Å). All bond lengths lie within the expected range, and relevant bond distances and angles are listed in Table 1. In the phenyl ring, the $C_{ar}-C_{ar}$ bond length between positions 5 and 6 is distinctly shorter (C2−C3: 1.366 Å and C15−C16: 1.361 Å) than those for the other five $C_{ar}-C_{ar}$ bonds. This observation is in agreement with significant contributions from resonance structures with the negative charge on the C atoms at positions 2 or 4 of the phenyl ring as well as on the N atoms of their −C≡N substituents: formally, the $C_{ar}-C_{ar}$bond between positions 5 and 6 holds, in all these cases, a double bond character. Furthermore, the C≡N bond lengths of the carbonitriles on the 1,1-dicyanoprop-2-en-1-ide moiety are perceptibly larger than those of the carbonitriles at the 2 and 4 positions of the phenyl ring, reflecting a more pronounced delocalization of the negative charge over the former unit. Accordingly, from the IR spectrum the stretching frequency ν(C≡N) at 2158 cm^{-1} can be assigned to the carbonitriles of the 1,1-dicyanoprop-2-en-1-ide group, whereas those of the carbonitrile groups directly bonding to the phenyl ring appear at 2179 and 2204 cm^{-1}.

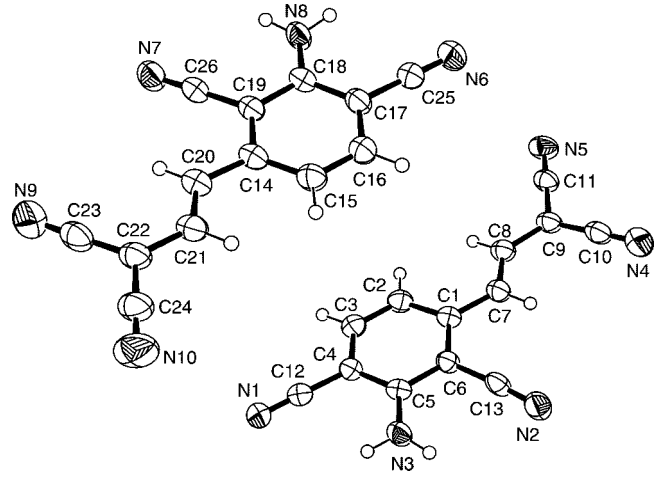

Figure 1. ORTEP drawings of the two anions of the asymmetric unit of **1**·0.5CH_3OH with thermal ellipsoids shown at 50% probability level.

The type of crystal packing is mainly determined by two factors: on the one hand by the information carried by the anions for a specific hydrogen bond donor/acceptor sequence which directs the association of these anions into an extended ribbon-type motif, and on the other hand by the ionic nature of the molecular units. First, we will address the distinct hydrogen bonding pattern. The 3-amino group of each anion acts as donor either to the 2- or to the 4-cyano acceptor group of two neighboring anions and consequently, these anions assemble into extended hydrogen-bonded zigzag chains. As a result, approximately 2 nm broad ribbon motifs extend along the *a*-axis (see Figure 2) exhibiting only a slight undulation in the *b*-direction (see Figure 3). Within these anionic ribbons, pairs of conventional hydrogen bonds link two adjacent anions, and hence, each anion is involved in four conventional hydrogen bonds. Altogether, these N−H···NC bonds exhibit four different donor···acceptor [N···N] distances in the range of 2.976−3.194 Å (see Table 2), which are somewhat shorter than those reported in the literature.[12] Furthermore, along the *c*-axis, these ribbons are arranged in a parallel and nearly coplanar fashion through further C−H···NC interactions. Consequently and most importantly, these extended and flat 2 nm broad ribbons represent structurally robust entities, which, while lying side by side, form negatively charged monomolecular layers. The tetrabutylammonium cations which are sandwiched between them balance

Table 1. Bond Lengths (Å) and Selected Bond Angles (°) for the Two Crystallographically Independent Anions of 1·0.5CH$_3$OH

N1−C12	1.151(3)	C1−C2	1.414(3)	C5−C6	1.421(3)
N2−C13	1.146(3)	C1−C7	1.442(3)	C6−C13	1.426(3)
N3−C5	1.353(3)	C2−C3	1.366(3)	C7−C8	1.358(3)
N4−C10	1.153(3)	C3−C4	1.402(3)	C8−C9	1.420(3)
N5−C11	1.152(3)	C4−C5	1.400(3)	C9−C10	1.412(4)
C1−C6	1.409(3)	C4−C12	1.425(3)	C9−C11	1.414(3)
N6−C25	1.148(3)	C14−C19	1.418(3)	C18−C19	1.414(3)
N7−C26	1.144(3)	C14−C20	1.443(3)	C19−C26	1.429(3)
N8−C18	1.357(3)	C15−C16	1.361(3)	C20−C21	1.359(3)
N9−C23	1.159(4)	C16−C17	1.403(3)	C21−C22	1.406(3)
N10−C24	1.154(4)	C17−C18	1.410(3)	C22−C23	1.390(4)
C14−C15	1.404(3)	C17−C25	1.424(3)	C22−C24	1.418(4)
C6−C1−C2	116.7(2)	C1−C6−C5	123.3(2)	N4−C10−C9	179.1(3)
C3−C2−C1	120.6(2)	C8−C7−C1	124.8(2)	N5−C11−C9	179.1(3)
C2−C3−C4	122.2(2)	C7−C8−C9	126.3(2)	N1−C12−C4	178.5(3)
C5−C4−C3	119.8(2)	C10−C9−C11	117.9(2)	N2−C13−C6	175.6(3)
C4−C5−C6	117.1(2)	H3A−N3−H3B	118(2)		
C15−C14−C19	117.3(2)	C18−C19−C14	122.7(2)	N9−C23−C22	177.6(3)
C16−C15−C14	121.4(2)	C21−C20−C14	124.4(2)	N10−C24−C22	178.9(4)
C15−C16−C17	121.1(2)	C20−C21−C22	126.6(2)	N6−C25−C17	179.3(3)
C16−C17−C18	120.8(2)	C23−C22−C24	118.3(2)	N7−C26−C19	178.9(3)
C17−C18−C19	116.7(2)	H8A−N8−H8B	116(2)		

the overall charge (Figure 3). The mean interlayer separation amounts to 7.76 Å (half the *b*-axis).

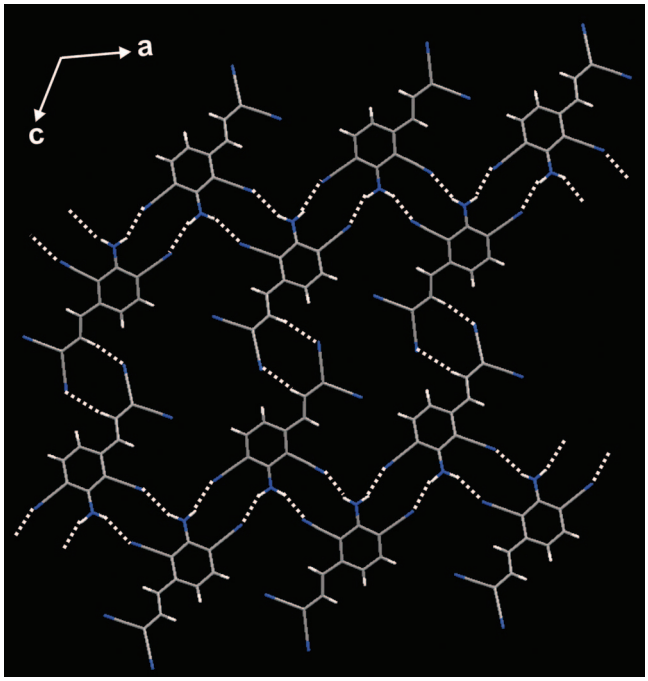

Figure 2. The *ac*-projection of the crystal structure (stick model) of compound **1**·0.5CH$_3$OH, illustrating a top-view of a molecular layer formed by the anions. A fragment of two hydrogen-bonded ribbons which run side by side along the *a*-axis is shown. The CH$_3$OH molecules are omitted for clarity.

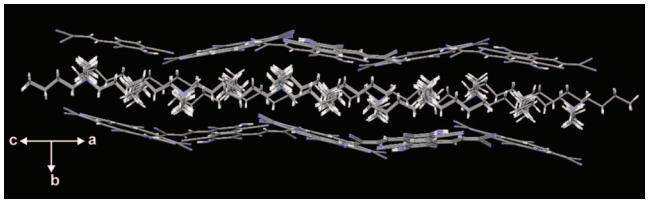

Figure 3. A projection along [101] of the crystal structure (stick model) of compound **1**·0.5CH$_3$OH, illustrating a side-view of the sandwich-type structure. The CH$_3$OH molecules are omitted for clarity.

Table 2. Selected Hydrogen-Bonding Parameters for 1·0.5CH$_3$OH

D−H···A	*d*(D−H), Å	*d*(H···A), Å	∠DHA, deg	*d*(D···A), Å
N3−H3A···N6	0.88(3)	2.15(3)	156(3)	2.976(4)
N3−H3B···N2	0.85(3)	2.35(3)	153(3)	3.124(3)
N8−H8A···N7	0.86(3)	2.37(3)	159(2)	3.194(4)
N8−H8B···N1	0.89(3)	2.26(3)	164(3)	3.119(3)
C8−H8···N10	0.95	2.51	166	3.442(4)
C21−H21···N5	0.95	2.55	170	3.491(4)

Optical Properties. The π-conjugated anion of **1** intensely absorbs in the visible region as evidenced by the orange-red color of the compound. Remarkably, the UV−vis solution spectrum (CH_2Cl_2) displays a very strong absorption band around 21 350 cm^{-1} (468.4 nm) with an extinction coefficient $\varepsilon = 8.5 \times 10^4$ L mol^{-1} cm^{-1} (Figure 4). Several additional absorption bands between 27 000 cm^{-1} and the UV region show extinction coefficients up to $\varepsilon = 3 \times 10^4$ L mol^{-1}cm^{-1}. Moreover, the chromophoric anion shows a Stokes-shifted (ν_{ST} = 2320 cm^{-1}) weak fluorescence emission at 19 030 cm^{-1} (525.5 nm) in dichloromethane solution at room temperature. The fluorescence excitation spectrum (ν_{em} = 18 868 cm^{-1}, λ_{em} = 530 nm) compares well with the corresponding absorption profile.

In order to understand the ground- and excited-state electronic properties of the π-conjugated anionic chromophore, density

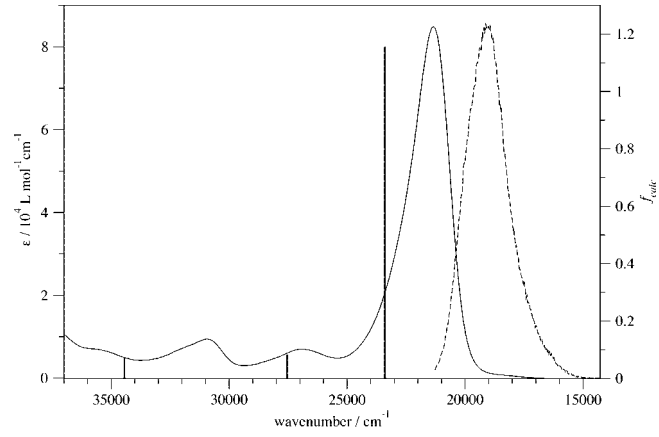

Figure 4. Electronic absorption (solid line) and emission fluorescence (dashed line; ν_{ex} = 21 739 cm^{-1}, λ_{ex} = 460 nm) spectra of **1** in deaerated dichloromethane solution at room temperature. Right-hand scale: calculated oscillator strength.

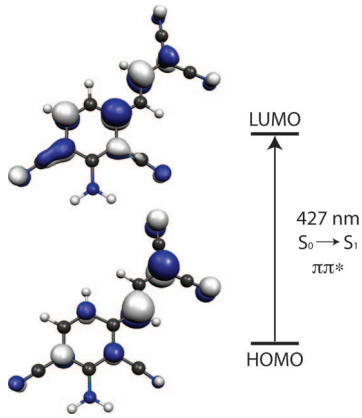

Figure 5. Molecular orbitals of the anion of **1** that are involved in the intramolecular $\pi-\pi^*$ transition; excitation from the HOMO to the LUMO.

Table 3. Absorption and Emission Maxima, A_{max} and E_{max}, Respectively, Stokes Shift ν_{ST}, and Luminescence Quantum Yield Φ_F of 1 in Different Solvents[a]

solvent	Δf	A_{max} [cm^{-1}]	E_{max} [cm^{-1}]	ν_{ST} [cm^{-1}]	Φ_F
CH_3OH	0.309	22300	19600	2700	0.02
CH_3CN	0.305	21790	19360	2430	0.02
CH_2Cl_2	0.217	21350	19030	2320	0.035
$CHCl_3$	0.148	21430	19380	2050	0.065

[a] Δf is the corresponding solvent polarity parameter.

functional (DFT) and time-dependent DFT (TD-DFT) methods were employed, as well as correlated ab initio calculations of excitation energies and response properties at the second-order coupled-cluster level, employing the resolution-of-the identity approximation (RICC2). All calculations were performed with the TURBOMOLE V5.9 program package.[13]

DFT and TD-DFT calculations were performed with the B3LYP functional and the TZVP basis set. The minimum-energy geometry is calculated to have C_s symmetry and the anionic skeleton is planar in both ground- and excited states. The vertical RICC2 calculations with the aug-cc-pVDZ basis set predict the $S_0 \rightarrow S_1$ electronic excitation to be an intense in-plane $\pi-\pi^*$ transition at 23 395 cm^{-1} (427 nm) with an oscillator strength $f_{calc} = 1.16$ (see the stick spectrum in Figure 4). Both the transition energy and the intensity are in acceptable agreement with the strong longest-wavelength absorption, for which the 19000−25000 cm^{-1} energy-integrated absorption yields an oscillator strength $f_{exp} = 0.84$. The $S_0 \rightarrow S_2$ excitation is predicted to be at 27 547 cm^{-1} (363 nm) with an oscillator strength $f_{calc} = 0.08$ and the $S_0 \rightarrow S_3$ transition at 34 441 cm^{-1} (290 nm) with $f_{calc} = 0.07$. Since the calculation does not take solvation effects into account, the calculated transition energies are blue-shifted with respect to the experimental ones. The $S_0 \rightarrow S_1$ excitation is dominated by the one-electron HOMO $\rightarrow$ LUMO contribution (88%). As Figure 5 shows, this electronic excitation mainly corresponds to a π-electron flow from the 1,1-dicyanoprop-2-en-1-ide substituent toward the dicyanoaniline moiety, and hence bears the characteristics of an intramolecular charge transfer (CT) transition. The dipole moments of the anion in the ground and the first electronically excited state, calculated at the RIMP2/aug-cc-pVDZ and the RICC2/aug-cc-pVDZ levels, respectively, are 9.54 Debye (S_0) and 5.63 Debye (S_1). Their vectors lie, as one may expect, in the direction of the longer molecule axis and point toward the 1,1-dicyanoprop-2-en-1-ide group (δ^- pole). Clearly, the intramolecular CT transition decreases the value of the dipole moment of the excited-state compared to that of the ground state.

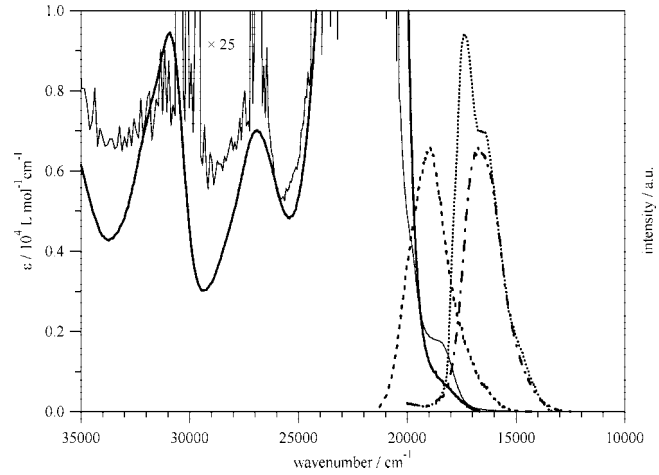

Figure 6. Electronic absorption spectra (solid line) and fluorescence emission (dashed line; $\nu_{ex} = 21\,739$ cm^{-1}, $\lambda_{ex} = 460$ nm) spectra of **1** in deaerated dichloromethane solution at room temperature, together with absorption spectrum at room temperature of a single crystal (thin solid line) as well as the solid state emission (dash-dots; $\nu_{ex} = 22\,222$ cm^{-1}, $\lambda_{ex} = 450$ nm) at room temperature and at 25 K (dots).

To obtain additional experimental information supporting the change of the dipole moment upon optical excitation, the solvent dependence of the optical spectra has been investigated and these data are summarized in Table 3. We use the Lippert-Mataga equation,[14,15] which expresses the Stokes shift as a function of the solvent polarity parameter Δf

$$\nu_{ST} = 2(\mu_e - \mu_g)^2 \frac{\Delta f}{hca^3} + C = 10070(\mu_e - \mu_g)^2 \frac{\Delta f}{a^3} + C \quad (1)$$

where Δf is calculated as[14]

$$\Delta f = \frac{(\varepsilon - 1)}{(2\varepsilon + 1)} - \frac{(n^2 - 1)}{(2n^2 + 1)} \quad (2)$$

and ε and n are the dielectric constant and the refractive index of the solvent, respectively. The Δf values for the series of solvents are included in Table 3. In eq 1, μ_e and μ_g are the dipole moments of the excited-state and the ground-state respectively, h is Planck's constant, c is the velocity of light, and a is the Onsager radius. The latter is set to 4.5 Å, as estimated from the crystallographic data of **1**, taking the radius of a sphere of the same volume as the estimated crystallographic volume for the anionic moiety of **1**. For the dipole moments in Debye and a in Å, the prefactor $2/(hc) = 10070$.[16] The Lippert-Mataga plot for **1** is shown in Figure S1, Supporting Information. From the slope of this plot, the difference of the dipole moments between the excited-state and the ground-state is estimated to be 5(1) Debye, in strikingly good agreement with the calculated values.

As a result of the quite unique and favorable crystal packing, where the π-conjugated anions are assembled and isolated within molecular monolayers, compound **1** exhibits upon photoexcitation at room temperature a solid state emission in the red part of the spectrum with a maximum at 17 360 cm^{-1} (576 nm). Figure 6 shows the solid state room temperature and low temperature emission spectra ($\nu_{ex} = 22\,222$ cm^{-1}, $\lambda_{ex} = 450$ nm). The solid state emission is red-shifted by an amount of 1670 cm^{-1} (vs emission in CH_2Cl_2 solution). The single crystal

Scheme 2. Angles Describing the Relative Orientation of the Electronic Transition Dipole Moments

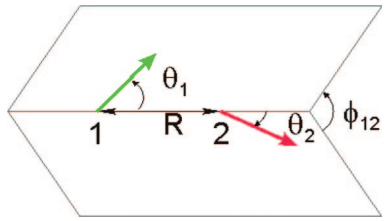

absorption spectrum is also depicted in Figure 6, but the crystal absorbs so intensely that only the basis of the absorption bands can be observed.

In the solid phase, resonant intermolecular interactions between the planar π-conjugated anions **1** result in the formation of Frenkel excitons, in which the excitation is shared between chromophores throughout the solid lattice. The resonant couplings can be estimated in the point dipole−point dipole interaction form,[6] which is based on the interaction between localized electronic transition dipole moments and neglects electronic overlaps of the π-systems of the individual chromophores. This approximation is appropriate if the intermolecular separations are larger than the molecular dimensions, which can still be considered as appropriate for the present case. We analyze the different resonant couplings in terms of contributions from the four unique pairs of molecular anions **1** in the lattice (see below). For each such pair, the S_1 excited-state is split into a higher and a lower energy level, quantified by the Davydov exciton splitting energy $\Delta E = 2\beta$, which depends on the interaction between the two electronic transition dipole moments μ_{AA^*}, eq 3, and their relative orientation, as expressed by the geometrical parameter κ_{AA^*} in eq 4:

$$\beta = \frac{1}{4\pi\varepsilon_0 n^2}\frac{|\mu_{AA*}|^2}{R^3}\kappa_{AA^*} \qquad (3)$$

$$\kappa_{AA^*} = \sin\theta_1 \sin\theta_2 \cos\varphi_{12} - 2\cos\theta_1 \cos\theta_2 \qquad (4)$$

R is the center of mass distance between two monomers, ε_0 is the vacuum permittivity, n the refractive index of the crystal, and θ_1, θ_2, and ϕ_{12} are the angles defined in Scheme 2.

The electronic transition dipole moment μ_{AA^*} can be expressed in terms of the oscillator strength f (eq 5):

$$f = \frac{8\pi^2 cm_e}{3he^2}\nu|\mu_{AA*}|^2 \qquad (5)$$

On the basis of the monomeric absorption spectrum of **1** in solution, with $f_{exp} = 0.84$, and setting the refractive index n to a reasonable value of 1.4, the interaction parameter β can be calculated as a function of the geometrical parameters. For instance, for an ideal in-line arrangement of two chromophores and their electronic transition dipole moments, the parameter κ_{AA^*} amounts to the limiting value of -2 and β remains as a function of R^{-3}. The crystal asymmetric unit gives rise to three unique pairs of neighboring anionic chromophores within an isolated layer.

Figure 7 shows three monomers, denoted A, B, and C, together with the calculated orientation of their $S_0 \rightarrow S_1$ electronic transition dipole moments. The A···B pair is close to an in-line geometry at a distance $R = 1.14$ nm; the resulting point dipole−point dipole $|\beta|$ interaction amounts to 280 cm^{-1}. The B···C pair is at a shorter distance $R = 1.04$ nm, but due to the angular term, $|\beta|$ amounts to 75 cm^{-1}. The A···C pair

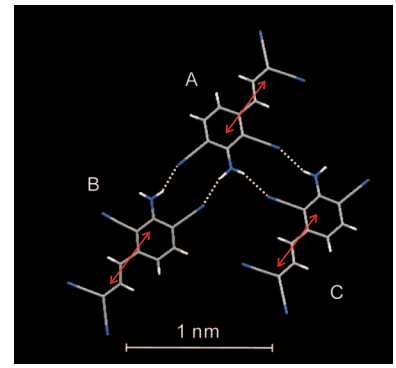

Figure 7. Structural arrangement of three chromophores within an isolated sheet showing the calculated orientation of their electronic transition dipole moments ($S_0 \rightarrow S_1$).

lies $R = 0.88$ nm apart, but due to unfavorable θ angles, the $|\beta|$ is only 85 cm^{-1}. In addition, along the *b*-axis, the shortest distance, for example, between chromophores A and A′ of neighboring anionic layers, measured at the C1 and C14 positions, is 0.85 nm. This brings the electronic transition moments into similar close contact as within the sheets, leading to a $|\beta|$ of 190 cm^{-1}. The hypsochromic absorption shifts associated with the A···C and A···A′ pairs are characteristic of so-called *H*-aggregates, whereas the bathochromic shifts for the A···B and B···C pairs are characteristic for more pronounced in-line arranged *J*-aggregates. Within the solid state, a complicated 3D excitonic band structure arises from the mutual couplings between all molecules. The simplified analysis given here already shows that the Davydov band splitting is dominated by the pairs A···B, followed by pairs formed via the neighboring layers. This order-of-magnitude estimate of the dominant contributions predicts that the excitonic delocalization not only takes place *within* the hydrogen-bonded monomolecular layers, but also between the sheets with a sizable amount.

Following absorption of light in the crystal, the excitons are rapidly thermalized via scattering with lattice phonons in a time much shorter than the fluorescence emission lifetime. Fluorescence emission proceeds from a thermal distribution of band-bottom excitons. The low-energy edge of the crystal absorption spectrum (Figure 6) shows a weak but distinct peak at 18 300 cm^{-1}. The maximum of the 25 K crystal fluorescence is about 940 cm^{-1} lower in energy (17 360 cm^{-1}). In defect-free crystals at low temperature, the intrinsic vibrationless 0−0 emission should display no Stokes shift, that is, the 0−0 emission must be identified with the maximum of the fluorescence band. This implies that the transitions from the low edge of the exciton band are optically forbidden. The weak 18 300 cm^{-1} band thus cannot be the 0−0 transition. We propose that it is due to an intramolecular vibrational transition, since the emission spectrum also exhibits a vibronic band spaced about 900 cm^{-1} from the maximum. Evidently, more detailed treatments would involve the consideration of the full 3D excitonic band structure as well as the electron−phonon coupling (dressed excitons), which is, however, beyond the scope of this paper.

Conclusions

This study has gone some way toward understanding several problem areas in the field of crystal engineering and materials properties. First, a specific synthetic route has been addressed which allows the preparation of a novel functional anionic molecule with remarkable photophysical properties, as very intense absorption features in the visible region with a high

oscillator strength, $f_{exp} = 0.84$, and fluorescence emission in solution and in the solid state. Second, the programming of these π-conjugated anions into a self-assembled 2D network through combined actions of hydrogen bonds and Coulombic interactions is embedded during the design and synthesis of the molecules, namely, through the specific sequence of hydrogen donor and acceptor substituents and through the resonance-stabilization of the molecule in its anionic (carbanionic) form. Third, the sandwich-type structure motif allows the realization of a rare case of spatially isolated molecular monolayers of these anionic chromophores within the crystalline state, which on the one hand suppresses a quenching of the solid state emission and on the other hand gives reliable geometrical parameters to probe the exciton states by the theoretical molecular exciton approximation.

Our ongoing studies clearly substantiate the concept of the spatially preorganized hydrogen bond donor/acceptor sequence built into the molecular skeleton of **1**. Even the incorporation of a sterically bulky trimethylsilyl group at 5-position of **1** preserves the formation of a planar extended ribbon-type motif within the resulting anionic sheets. Moreover, the exchange of tetrabutylammonium with Oxazine 1 cations keeps the layered assembly intact which underlies the robustness of the overall motif.[17]

Acknowledgment. This work was supported by the Swiss National Science Foundation (grant No. 200020-116003 and COST Action D31).

Supporting Information Available: X-ray crystallographic information file (CIF) and the Lippert-Mataga plot are available for **1**. This material is available free of charge via the Internet at http://pubs.acs.org.

References

(1) (a) *Perspectives in Supramolecular Chemistry*; Desiraju, G. R., Ed.; Wiley: Chichester, 1996; Vol. 2. (b) *Topics in Current Chemistry - Supramolecular Dye Chemistry*; Würthner, F., Ed.; Springer-Verlag: Berlin, 2005; Vol. 258. (c) Steed, J. W.; Atwood, J. L. *Supramolecular Chemistry*; John Wiley & Sons: Chichester, 2000. (d) Desiraju, G. R. *Crystal Engineering: The Design of Organic Solids;* Elsevier: New York, 1989. (e) Lindoy, L. F.; Atkinson, I. M. *Self-Assembly in Supramolecular Systems*; Royal Society of Chemistry: Cambridge, 2000. (f) Desiraju, G. R. *Angew. Chem., Int. Ed.* **2007**, *46*, 8342.

(2) (a) Paz, F. A. A.; Klinowski, J. *CrystEngComm* **2003**, *5*, 238. (b) Aakeröy, C. B.; Schultheiss, N.; Desper, J.; Moore, C. *Cryst. Growth Des.* **2007**, *7*, 2324. (c) Dalrymple, S. A.; Shimizu, G. K. H. *J. Am. Chem. Soc.* **2007**, *129*, 12114. (d) Sansam, B. C. R.; Anderson, K. M.; Steed, J. W. *Cryst. Growth Des.* **2007**, *7*, 2649.

(3) (a) Xue, F.; Mak, T. C. W. *J. Phys. Org. Chem.* **2000**, *13*, 405. (b) Martin, S. M.; Yonezawa, J.; Horner, M. J.; Macosko, C. W.; Ward., M. D. *Chem. Mater.* **2004**, *16*, 3045. (c) Nicoud, J.-F.; Masse, R.; Bourgogne, C.; Evans, C. *J. Mater. Chem.* **1997**, *7*, 35. (d) Russell, V. A.; Ward, M. D. *J. Mater. Chem.* **1997**, *7*, 1123. (e) Turner, D. R.; Pek, S. N.; Batten, S. R. *Chem. Asian J.* **2007**, *2*, 1534. (f) Xie, J.; Ma, M. T.; Abrahams, B. F.; Wedd, A. G. *Inorg. Chem.* **2007**, *46*, 9027. (g) Yoshikawa, I.; Sawayama, J.; Araki, K. *Angew. Chem., Int. Ed.* **2008**, *47*, 1038.

(4) (a) Jia, C.; Liu, S.-X.; Tanner, C.; Leiggener, C.; Neels, A.; Sanguinet, L.; Levillain, E.; Leutwyler, S.; Hauser, A.; Decurtins, S. *Chem. Eur. J.* **2007**, *13*, 3804. (b) Goze, C.; Leiggener, C.; Liu, S.-X.; Sanguinet, L.; Levillain, E.; Hauser, A.; Decurtins, S. *ChemPhysChem* **2007**, *8*, 1504. (c) Jia, C.; Liu, S.-X.; Tanner, C.; Leiggener, C.; Levillain, E.; Leutwyler, S.; Hauser, A.; Decurtins, S. *Chem. Commun.* **2006**, 1878. (d) Rusanova, J.; Decurtins, S.; Rusanov, E.; Stoeckli-Evans, H.; Delahaye, S.; Hauser, A. *J. Chem. Soc., Dalton Trans.* **2002**, 4318.

(5) (a) Busse, G.; Frederichs, B.; Petrov, N. Kh.; Techert, S. *Phys. Chem. Chem. Phys.* **2004**, *6*, 3309. (b) Kometani, N.; Nakajima, H.; Asami, K.; Yonezawa, Y.; Kajimoto, O. *J. Phys. Chem. B* **2000**, *104*, 9630. (c) Kroon, J. M.; Koehorst, R. B. M.; van Dijk, M.; Sanders, G. M.; Sudhölter, E. J. R. *J. Mater. Chem.* **1997**, *7*, 615.

(6) (a) Kasha, M.; Rawis, H. R.; El-Bayoumi, M. A. *Pure Appl. Chem.* **1965**, *11*, 371. (b) Rashba, E. I.; Sturge, M. D. *Excitons*; North-Holland: Amsterdam, 1982. (c) Broude, V. B.; Rashba, E. I. *Spectroscopy of Molecular Excitons*; Springer-Verlag: Berlin, 1985. (d) Davydov, A. S. *Theory of Molecular Excitons*; Plenum: New York, 1971. (e) Agranovich, V. M.; Hochstrasser, R. M. *Spectroscopy and Excitation Dynamics of Condensed Molecular Systems*; Elsevier: Amsterdam, 1983. (f) Würthner, F.; Yao, S.; Debaerdemaeker, T.; Wortmann, R. *J. Am. Chem. Soc.* **2002**, *124*, 9431.

(7) (a) Ooyama, Y.; Mamura, T.; Yoshida, K. *Tetrahedron Lett.* **2007**, *48*, 5791. (b) Ooyama, Y.; Yoshikawa, S.; Watanabe, S.; Yoshida, K. *Org. Biomol. Chem.* **2007**, *5*, 1260.

(8) (a) Bowling, N. P.; Mcmahon, R. J. *J. Org. Chem.* **2006**, *71*, 5841. (b) Yi, C.; Blum, C.; Liu, S.-X.; Frei, G.; Neels, A.; Renaud, P.; Leutwyler, S.; Decurtins, S. *J. Org. Chem.* **2008**, *73*, 3596.

(9) *Stoe & Cie. X-Area V1.35 & X-RED32 V1.31 Software*; Stoe & Cie GmbH: Darmstadt, Germany, 2006.

(10) Sheldrick, G. M. *Acta Crystallogr.* **2008**, *A64*, 112.

(11) Spek, A. L. *J. Appl. Crystallogr.* **2003**, *36*, 7.

(12) (a) Pandi, A. S.; Velmurugan, D. V.; Shanmuga, S.; Raj, S.; Fun, H-K.; Raghukumar, V.; Ramakrishnan, V. T. *Acta Crystallogr.* **2001**, *C57*, 723. (b) Custelcean, R. *Chem. Commun.* **2008**, 295.

(13) (a) Ahlrichs, R.; Bär, M.; Häser, M.; Horn, H.; Kölmel, C. *Chem. Phys. Lett.* **1989**, *162*, 165. (b) Treutler, O.; Ahlrichs, R. *J. Chem. Phys.* **1995**, *102*, 346. (c) Hättig, C.; Weigend, F. *J. Chem. Phys.* **2000**, *113*, 5154. (d) Weigend, F.; Häser, M. *Theor. Chem. Acc.* **1997**, *97*, 331.

(14) Sumalekshmy, S.; Gopidas, K. R. *J. Phys. Chem. B* **2004**, *108*, 3705.

(15) Mataga, N.; Kaifu, Y.; Koizumi, M. *Bull. Chem. Soc. Jpn.* **1956**, *29*, 465.

(16) Lauteslager, X. Y.; van Stokkum, I. H. M.; van Ramesdonk, H. J.; Bebelaar, D.; Fraanje, J.; Goubitz, K.; Schenk, H.; Brouwer, A. M.; Verhoeven, J. W. *Eur. J. Org. Chem.* **2001**, 3105.

(17) Figures S2 and S3 show the formation of a planar extended ribbon-type motif leading to a sandwich-type structure (see Supporting Information).

CG800122V